4

FERROCENE BILAYERS ON ITO FOR HYBRID PEROVSKITE SOLAR CELLS

Abstract: *This chapter investigates the synthesis of 4-aminobutylferrocene hydroiodide, the hurdles in synthesizing it as well as using Self-Assembled Bilayers (SABs) formed from* ***FcPA*** *(**Chapter 2**) and 4-aminofbutylferrocene hydroiodide for hybrid perovskite solar cells.*

I would like to thank and acknowledge Javier E. Sebastián Alonso for his help with the fabrication and measurement of the solar cells.

4.1. INTRODUCTION

In the last 15 years, the efficiency of hybrid perovskites solar cells has gone up from 3.8 % to close to 26 %.[1,2] Even though the performance of solar cells has increased significantly in the last decade problems of interface recombination, grain boundaries, moisture degradation and ion migration still hinder the field.[3–5] To tackle the interface recombination, moisture degradation and ion migration researchers started implementing surface passivation utilizing different ammonium salts.[6,7] The ammonium salts help with passivation of the surface, increasing the size of the grains and lowering the interface recombination. Simple molecules such as ethylamines,[8,9] butylamine[10] to aromatic amines such as phenylethylamine[11–13] and thiophene[14–18] based amines have been used. Crystal growth conditions determine whether a bulk or 2D hybrid perovskite is obtained. The use of the Ruddlesden-Popper structure is prevalent in applying 2D perovskites in solar cells.

Zhao *et al.* investigated the effect of steric hindrance of the spacer cation butylammonium iodide on the performance of solar cells. By comparing the effect of the steric hindrance of the isomers n-butylammonium iodide, i-butylammonium iodide, and tert-butylammonium iodide on the performance of the solar cells, the authors show an inversely proportional trend. The decrease in performance is directly correlated with an increase in hindrance. This is due to the decrease in the diffusion of butylammonium iodide to grain boundaries, resulting in a negative impact on passivation and hole transport.[19] Aromatic ammonium salts are commonly used to aid with the charge transfer between layers of the hybrid perovskites. In principle, due to π-π interactions and stacking, the aromatic spacer aids with obtaining higher order of crystallinity which promotes charge transfer between the layers of the perovskites.[20,21] One aromatic compound frequently used is the phenylethylammonium (PEA) halide. Using transient transmission and reflection microscopy Wang *et al.* showed that PEAI can enhance charge carrier density at the near-surface and reduce the defect density by a whole order of magnitude.[22] Furthermore, Zhang *et al.* showed that using molecular design and fluorinating the phenyl ring in the para position increases the PCE from 9.66 % to 13.64 % and enhances the thermal stability of the devices.[13]

Commonly employed core material in a variety of semiconducting polymers specifically designed for use in organic solar cells is thiophene.[23–25] Among these polymers, P3HT has been the subject of extensive research, and has emerged as the most widely investigated. Notably, researchers have recently employed P3HT as a passivating layer, which has resulted in certified power conversion efficiency (PCE) values of 22.7 % over the past years.[26–29] Researchers have been exploring the use of thiophene for hybrid perovskite solar cells. In their research, Du *et al.* found that using 2-thiopheneethylammonium iodide (TEAI) to create 2D/3D perovskite resulted in improved characteristics and stability compared to the 3D device without TEAI,[16] which is consistent with previous findings.[14,16] Similarly, when TEAI was used to fabricate full 2D perovskite, Xu *et al.* achieved a 6.8 % PCE for $MASnI_3$.[15] However, directionality of 2D perovskites was found to matter for device performance, as devices made with only thiophenemethylammonium iodide (ThMAI) had low PCE due to low crystallinity and random orientation. Adding MACl as an additive in the precursor solution led to an increase in crystallinity and formation of a nanorod-like structure, resulting in a drastic

increase of PCE from 1.74 % to 15.42 % for devices using MACl.[17]

In order to tackle any potential complications that may arise from utilizing small spacer molecules during crystal growth, we have reevaluated alternative options that can function as efficient spacers. Here we report the first use of ferrocenylbutylammonium iodide. When designing the cationic spacer, we chose ferrocene as the core due to its known stable organometallic compound with very well-known chemistry[30–32] and the redox potential of –0.40 V.[33,34] Furthermore, we considered the length of the alkyl chain needed to decouple the molecular orbitals of ferrocene from pinning to the electronic levels of the electrodes.[35–38] It is important to separate the electronic levels of the electrodes from the molecular orbitals to prevent any undesired shifts that can affect charge transport. Recent research on molecular junctions using the polarizable ferrocene moiety has shown that the direction of rectification depends on the position of the ferrocene and its proximity to the electrodes.[39–42] Yuan *et al.* have demonstrated the ability to switch the direction of rectification by adjusting the position of the ferrocene moiety in the molecular junction.[43] 4-Ferrocenylbutylphosphonic acid (**FcPA**) was utilized to form a covalent monolayer on top of the ITO substrate (the synthesis of **FcPA** is reported in Chapter 2). Furthermore, 4-aminobutylferrocene hydroiodide (**4**) was employed as a dynamic self-assembled monolayer in a self-assembled bilayer. The effectiveness of this approach was demonstrated by fabricating solar cells in a p-i-n device architecture, with $Cs_{0.25}FA_{0.75}Sn_{0.5}Pb_{0.5}I_3$ serving as the active layer and C_{60} and Ag as the top electrode.

4.2. RESULTS & DISCUSSION

We began synthesizing 4-aminobutylferrocene hydroiodide (**Scheme 4.1**) by Friedel-Crafts acylation of ferrocene with 4-chlorobutylroyl chloride. We obtained the product 4-chlorobutyrylferrocene (**1**) with a yield of 71 %. The limited yield is due to the chemical equivalence of the two cyclopentadiene rings. To prevent double acylation we added 1 equivalent of 4-chlorobutyryl chloride dropwise and stirred the reaction vigorously.

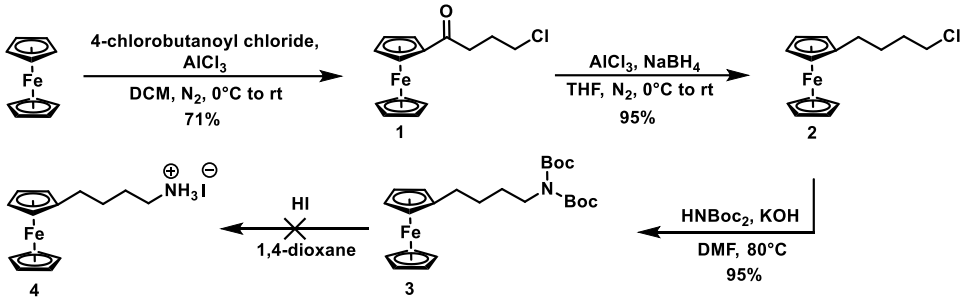

Scheme 4.1 Reaction scheme for synthesis of 4-aminobutylferrocene hydroiodide (**4**). Acetylating ferrocene via Friedel-Crafts acylation to obtain **1**, followed by reduction of the ketone group using $AlCl_3$ and $NaBH_4$ and reacting further with $HNBoc_2$ to obtain **3.**

$NaBH_4$ on its own reduces aldehydes to primary alcohols and ketones to secondary alcohols but not to alkanes leaving the desired intermediate 4-chlorobutyrylferrocene **2** unobtainable. A way to reduce ketones to alkanes is by using hydrazine under basic con-

ditions at high temperatures, a reaction known as Wolf-Kishner reduction. Regrettably, the conditions for substrate **1** may be too severe. However, there is a more gentle reaction condition available, which involves using $NaBH_4$ and $AlCl_3$ as a reagent. This method was first reported by Brown *et al.* in 1955,[44] and was also utilized by Mohammad-Pour *et al.* on a similar substrate to ours to convert ketone to alkane.[45] The first step of the mechanism of reducing the ketone to the alkane (**Scheme 4.2**) is the formation of the oxonium cation of the substrate and $AlCl_3$ via the free electron pair on the oxygen. The second step is the formation of the net neutral charge species by a nucleophilic attack by a hydride on the carbon and elimination of a chloride from the $AlCl_3$ moiety. A second subsequent nucleophilic attack from another hydride reduces the carbon atom, eliminates a chloride and Al(O)Cl as products and we obtain the desired alkane. Using only $NaBH_4$ or $LiAlH_4$ will result only in the secondary alcohol.[46–48]

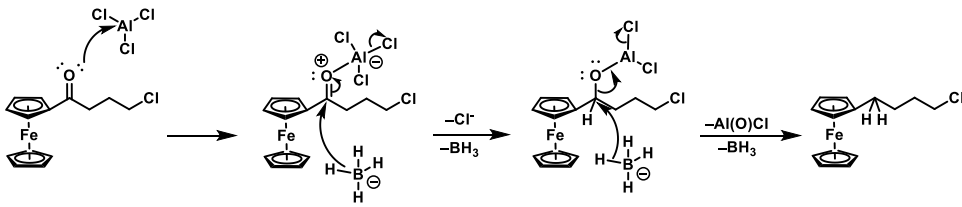

Scheme 4.2 Proposed reaction mechanism for reduction of ketone to alkane using $AlCl_3$ and $NaBH_4$ by formation of the oxonium species with $AlCl_3$ followed by nucleophilic attack by hydride resulting in neutral charge species and a second hydride attack to fully reduce the starting material to **2**

An additional proof of the incompatibility of substrate **1** with the reaction conditions of the Wolf-Kishner reduction is the test reaction of hydrolysis of the chloride **1** to the primary alcohol under basic conditions. Rather than obtaining the desired alcohol, we obtained cyclopropane product. Under basic conditions, KOH deprotonates the α protons promoting the enolate ion's formation. Rotation of the single bond between the α and β carbon brings the γ carbon closer to α carbon, making the formation of the cyclopropane product **5** a possibility (**Scheme 4.3**).

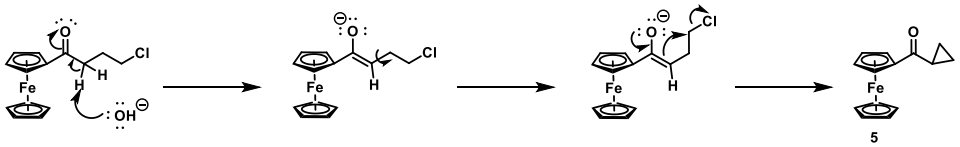

Scheme 4.3 Proposed reaction mechanism for formation of **5** under basic condition occurring via a deprotonation of α carbon, bond rotation, and elimination of a chloride.

Converting the alkyl chloride **2** to the doubly Boc-protected amine **3** is a straightforward high yielding S_N2 reaction. The justification behind using a doubly Boc-protected amine as our starting point for obtaining the ammonium iodide salt **4** is the formation of the ammonium salt during Boc-deprotection using acids. All of our attempts to synthesize the ammonium iodide **4** using 57 wt% HI failed. The reaction mixture usually turns into dark red/black tar, and neither the starting material nor the

product is obtained. It is believed that the starting material decomposes because of the acid-catalyzed oxidation of ferrocene into ferrocenium, which is then followed by the decomposition of the compound.[49–53]

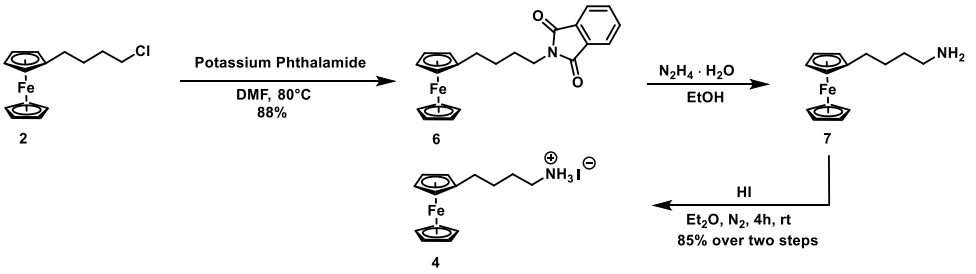

Scheme 4.4 Synthesis of the desired product **4** via Gabriel synthesis of primary amines by reacting **2** with potassium phthalimide, reacting it with hydrazine to obtain the free amine **6** and reacting it with HI to obtain the desired product **4**.

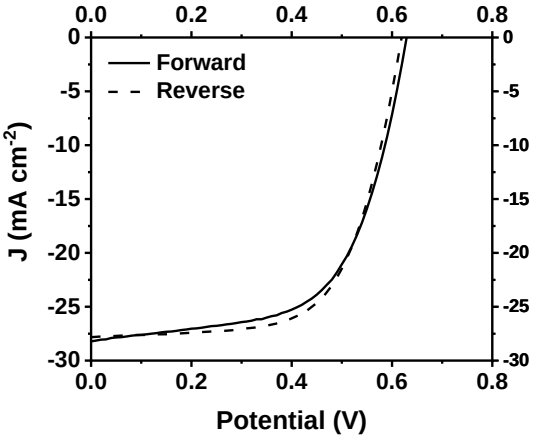

Figure 4.1 J-V curves of solar cell device under forward and reverse bias using SAB.

The inaccessibility of the desired product **4** prompted us to look into alternative synthetic pathways. Converting alkyl halides into primary amines can be done via Gabriel synthesis of primary amines using potassium phthalimide and hydrazine. The first step is a S_N2 substitution of the chloride to the phthalimide to obtain 4-phthalamidylbutylferrocene **6** in 88 % yield. **6** was suspended in EtOH followed by the addition of hydrazine monohydrate solution ($N_2H_4 \cdot H_2O$). The reaction mixture was refluxed for 4 hours to obtain the free amine. Immediately after the work up, the free amine was set up for the following reaction. A Schlenk tube under an inert atmosphere was charged with **7** and dissolved in anhydrous Et_2O. A three-neck flask charged with KI and dropwise addition of H_3PO_4 (10 mL) was gently heated to promote the formation of HI gas that was ran through drying agent (P_2O_5) before bubbling it through the reaction solution. The reaction was monitored by following the precipitate formation and discoloration of the solution from yellow/orange to colorless. The product was washed under an inert atmosphere with anhydrous Et_2O and dried on Schlenk line **Scheme 4.4**.

To prepare the ITO substrates, we used a standard cleaning process which involved

Bias	J_{sc} ($mA\,cm^{-2}$)	V_{oc} (V)	FF	PCE (%)
Forward	28.22	0.63	0.61	10.79
Reverse	27.82	0.62	0.65	11.14

Table 4.1 Photovoltaic parameters using ferrocene-based SAB as charge injection layer for mixed perovskites solar cell

scrubbing, ultrasonication in water, acetone, isopropanol, drying in the oven, and exposure to UV$-O_3$. The prepared substrates were dipped overnight in a 0.1 mM solution of **FcPA**. The next day, the excess of **FcPA** was removed by spinning them at 3000 rpm for 30 seconds and washing with 200 µL every 10 seconds and annealing at 100 °C for 1 minute. To form the SAB, the monolayer was covered with a 0.1 mM solution of the 4-aminobutylferrocene hydroiodide. After being left for 1 to 2 minutes, the sample was spun at 3000 rpm and annealed at 100 °C for 1 minute. 100 µL of $Cs_{0.25}FA_{0.75}Sn_{0.5}Pb_{0.5}I_3$) was spin coated and 250 µL was added during spin coating. Afterwards the sample was annealed at 120 °C for 10 minutes prior to deposition of C_{60}, BCP, and Ag as a top electrode. Under both forward and reverse bias, the device showed a small hysteresis (**Figure 4.1**), with J_{sc} measuring at 28.22 $mA\,cm^{-2}$ and 27.82 $mA\,cm^{-2}$, respectively. Additionally, the values for Voc and FF were alike (**Table 4.1**).

4.3. CONCLUSION

We have successfully synthesized 4-aminobutylferrocene hydroiodide, but encountered difficulties in synthesizing the target molecule **4** (**Scheme 4.1**). This report is significant because the method of producing ammonium iodide using Boc-protected amines and 57 % HI solutions did not work. Our research revealed that the decomposition of ferrocene to ferrocenium via acid catalyzed oxidation followed by decomposition was the primary cause of the issue. To prevent this, we recommend synthesizing the free amine through Gabriel synthesis and bubbling dry HI gas under an inert atmosphere.

As a proof of concept, we created a charge injection layer. We used 4-aminobutylferrocene hydroiodide and ferrocenylbutylphosphonic acid to form SABs on the ITO surface and used it to make a solar cell with $Cs_{0.25}FA_{0.75}Sn_{0.5}Pb_{0.5}I_3$as the active layer, C_{60} and Ag as the top electrode. The devices showed minimal hysteresis when operating under forward and reverse bias, but the PCE values of around 11 % indicate that there is still room for improvement. Further optimization in the fabrication process is needed to achieve higher values.

4.4. EXPERIMENTAL

All reagents were purchased from Sigma-Aldrich, Acros, TCI Europe and used as received unless otherwise stated. Anhydrous THF, DMF were obtained from an in-house Solvent Purification System. For thin layer chromatography (TLC) Merc silica gel 60 F_{254} aluminium plates were used. Visualization of compounds by TLC were done by irradiation with UV light, I_2, $KMnO_4$ or PMA stain. Column chromatography was performed using a Silicagel Kieselgel 60 M(0.04 – 0.063 mm, 230 – 400 mesh). ^{1}H NMR, ^{13}C NMR were performed on Agilent Technologies 400/54 Premium Shielded (400MHz), Varian Oxford AS400 (400MHz) nuclear magnetic resonance spectrometer. The following abbreviations were used to explain NMR peak multiplicities: s = singlet, d = doublet, t = triplet, q = quartet, m = multiplet, br = broad. High resolution mass spectra (HRMS) was recorded on Thermo Scientific LTQ Orbitrap XL (ESI^+, ESI^-, APCI).

4-chlorobutyrylferrocene (1) A Schlenk tube was charged with ferrocene (5 g), $AlCl_3$ (4.3 g, 32.3 mmol, 1.2 eq.) and anhydrous CH_2Cl_2 (50 mL) under inert N_2 atmosphere. The solution was cooled down to 0 °C prior to dropwise addition 4-chlorobutyryl chloride. After the addition of the reagent the reaction mixture was allowed to reach room temperature and was stirred overnight. The reaction was quenched the following day using 1 N solution of HCl, extracted with CH_2Cl_2, washed with water, brine and dried over $MgSO_4$. The solvent was removed under reduced pressure. The crude mixture was purified using silica chromatography using Pentane:EtOAc (90:10 v/v %) to obtain the desired product as orange solid (5.558 g, yield 71 %).

^{1}H NMR (400 MHz, $CDCl_3$) δ 4.9 – 4.8 (m, 2H), 4.6 – 4.5 (m, 2H), 4.2 (s, 5H), 3.7 (t, J = 6.1 Hz, 2H), 2.9 (t, J = 6.9 Hz, 2H), 2.2 – 2.1 (m, 2H). ^{13}C NMR (101 MHz, $CDCl_3$) δ 203.3, 72.4, 70.0, 69.4, 45.0, 36.1, 26.9. HRMS - ESI^+ (m/z) Calculated for $C_{14}H_{16}Cl_1FeO$ $[M+H]^+$: 291.02336 Measured: 291.02309

4-chlorobutylferrocene (2) A Schlenk tube was charged with 4-chlorobutyrylferrocene (5.56 g, 19.1 mmol), $AlCl_3$ (3.06 g, 22.9 mmol, 1.2 eq.) and anhydrous THF (90 mL) under inert N_2 atmosphere. The solution cooled down to 0 °C prior to portion-wise addition of $NaBH_4$ (2.17 g, 57.4 mmol. After the addition of $NaBH_4$ the reaction mixture was left to warm up to room temperature and left to react overnight. The reaction was quenched the following day using 1 N solution of HCL extracted with CH_2Cl_2, washed with water, brine and dried over $MgSO_4$. The solvent was removed under reduced pressure. The crude mixture was purified using silica chromatography and pentane:EtOAc (98:2 v/v %) as eluent to obtain the product as orange oil (5.02 g, yield 95 %).

^{1}H NMR (400 MHz, $CDCl_3$) δ 4.1 (d, J = 18.2 Hz, 9H), 3.5 (t, J = 6.6 Hz, 2H), 2.4 (t, J = 7.7 Hz, 2H), 1.8 (p, J = 7.1 Hz, 2H), 1.6 (p, J = 7.8 Hz, 2H). ^{13}C NMR (101 MHz, $CDCl_3$) δ 91.3, 71.2, 70.7, 69.9, 47.6, 35.0, 31.5, 30.9.

4-phthalamidylbutylferrocene (6) A 250 mL flask was charged with 4-chlorobutyrylferrocene (5.02 g, 18.2 mmol) and potassium phthalimide (6.72 g, 36.3 mmol, 2 eq.)and DMF (40 mL), heated to 80 °C and left stirring overnight. The reaction was worked up the following day using 10 % solution of LiCl, extracted with

EtOAc, washed with water, brine and dried over $MgSO_4$. The solvent was removed under reduced pressure. The crude mixture was purified by silica chromatography with pentane:EtOAc (90:10 v/v %).

^{1}H NMR (400 MHz,$CDCl_3$) δ 7.8 (dd, J = 5.4, 3.1 Hz, 2H), 7.7 (dd, J = 5.5, 3.0 Hz, 2H), 4.1 (s, 5H), 4.0 (d, J = 1.8 Hz, 2H), 4.0 (d, J = 1.9 Hz, 2H), 3.7 (t, J = 7.2 Hz, 2H), 2.4 (t, J = 7.7 Hz, 2H), 1.7 (p, J = 7.4 Hz, 2H), 1.6 (d, J = 4.8 Hz, 3H). HRMS - ESI$^+$ (m/z) Calculated for $C_{22}H_{21}FeNO_2$ $[M]^+$: 387. 09217 Measured: 387.09147

4-aminobutylferrocene (7) A 250 mL flask was charged with N-(4-phathalamideylbutylferrocene (1.5 g, 3.9 mmol), EtOH (72 mL, followed by addition of hydrazine monohydrate (50 to 60 wt% solution, 20 mL) and heated to reflux for 4 hours. The solution was cooled down to room temperature and EtOH was removed under reduced pressure, extracted with Et_2O, washed with water, brine and dried over $MgSO_4$. The product (orange oil) was used right away for the synthesis of 4-ferrocenylammonium iodide.

^{1}H NMR (400 MHz, CD_2Cl_2) δ 4.1 (s, 5H), 4.1 (t, J = 1.8 Hz, 2H), 4.0 (t, J = 1.8 Hz, 2H), 2.7 (t, J = 6.8 Hz, 2H), 2.3 (t, J = 7.5 Hz, 3H), 2.2 – 1.9 (m, 2H), 1.6 – 1.4 (m, 4H). ^{13}C NMR (101 MHz, CD_2Cl_2) δ 89.6, 68.8, 68.7, 68.4, 67.4, 42.3, 33.9, 30.5, 29.8, 28.8. HRMS - ESI$^+$ (m/z) Calculated for $C_{14}H_{20}FeN$ $[M+H]^+$: 258.09397 Measured: 258.09355

4-aminobutylferrocene hydroiodide (4) A Schlenk tube was charged with 4-ferrocenylbutylamine and anhydrous Et_2O (30 mL). After stirring for 5 minutes, dry in-situ generated HI was bubbled through the solution. Bubbling of HI was stopped when the solution discolored. The precipitate was washed with anhydrous Et_2O under N_2 and dried on Schlenk line to obtain the product as orange solid (1.26 g, yield 85% over two steps).

^{1}H NMR (400 MHz, DMSO-d6) δ 7.5 (s, 3H), 4.1 (s, 5H), 4.1 (t, J = 1.8 Hz, 2H), 4.0 (t, J = 1.8 Hz, 2H), 2.8 (t, J = 7.1 Hz, 2H), 2.3 (t, J = 7.1 Hz, 2H), 1.6 – 1.4 (m, 4H). ^{13}C NMR (101 MHz, DMSO-d6) δ 88.3, 68.3, 67.8, 66.9, 28.5, 27.4, 27.0. HRMS - ESI$^+$ (m/z) Calculated for $C_{14}H_{20}FeN$ $[M+H]^+$: 258.09397 Measured: 258.09411 HRMS - ESI$^-$ (m/z) Calculated for I^- $[M]^-$: 126.90502 Measured: 126.90573

N,N-di(tert-butoxycarbamyl)-4-aminobutyl ferrocene (3) A 100 mL flask was charged with KOH (0.53 g, 9.38 mmol, 1.5 eq.), $HNBoc_2$ (2.6 g, 9.38 mmol, 1.5 eq.) and DMF (10 mL). After 30 minutes 4-chlorobutylferrocene (1.73 g, 6.25 mmol) and additional DMF (10 mL) was added and stirred at 80 °C overnight. The following the reaction mixture was added to 10 % solution of LiCl, extracted with EtOAc, washed with water, brine and dried over $MgSO_4$. The solvent was removed under reduced pressure. The crude mixture was purified using silica chromatography using pentane:EtOAc (90:10 v/v %). The product was obtained as orange solid (2.71 g, 95 % yield).

^{1}H NMR (400 MHz, $CDCl_3$) δ 4.1 (s, 5H), 4.1 (d, J = 7.1 Hz, 4H), 3.6 (t, J = 7.3 Hz, 2H), 2.3 (t, J = 7.6 Hz, 2H), 1.6 – 1.5 (m, 2H), 1.5 (s, 20H). Note: Singlet @ 1.5 is singlet and a triplet overlapping. ^{13}C NMR (101 MHz, $CDCl_3$) δ 153.2, 89.7, 82.5, 69.1, 68.6, 67.7, 46.7, 29.7, 29.4, 28.6, 28.5. HRMS - ESI$^+$ (m/z) Calculated for $C_{12}H_{35}FeNNaO_4$ $[M+Na]^+$: 480.18077 Measured: 480.18044

PEROVSKITE PRECURSOR SOLUTION ($Cs_{0.25}FA_{0.75}Sn_{0.5}Pb_{0.5}I_3$)
The precursor solution was prepared in a vial by mixing CsI (181.86 mg, 0.7 mmol) FAI (361.2 mg, 2.1 mmol), PbI_2 (645.42 mg, 1.4 mmol) SnI_2 (521.6 mg, 1.4 mmol) followed by addition of 2 mL of DMF:DMSO (4:1 v/v% ratio) and stirring overnight. SnF_2 (0.14 mmol was added as additive to retard the oxidation of Sn^{2+} to Sn^{4+}. Prior to deposition the stirred solution was filtered using 0.20 µm PTFE filter.

DEVICE FABRICATION
Devices were fabricated on $30\,mm^2 \times 30\,mm^2$ prepatterned indium tin oxide (ITO) coated glass substrates that were ultrasonically cleaned in detergent solution, deionized water, acetone and isopropanol. After drying them in oven at 140 °C for 10 m to 20 minutes the substrates were treated with UV-O_3 for 20 minutes. The monolayer was formed by dipping the cleaned substrates in an 0.1 m M solution of **FcPA** in EtOH that was ultrasonicated for 30 minutes. The following day the substrates were spun for 10 s at 3000 rpm for 30 seconds and washed with 200 µL of EtOH before going on a hot plate at 100 °C for 1 minute. The formation of SABs was completed by covering the samples with the monolayer with $0.5\,mg\,mL^{-1}$ solution of **4** left for 1 m to 2 minutes prior to spinning the sample at 3000 rpm and dried at 100 °C to 120 °C for 1 m to 5 minutes. 100 µL of the active material was spincoated at 4000 rpm for 80 s and at 25 s 250 µL of anisole was added. The sample was heated at 120 °C for 10 minutes. Finally, deposition of C_{60} (20 nm), BCP (6 nm) and Ag (100 nm as the top electrode).

CURRENT DENSITY-VOLTAGE (J-V) MEASUREMENTS
J-V curves were recorded using Keithley 2400 source-meter under simulated *AM 1.5 G* solar illumination using a Steuernagel Solar constant 1200 metal halide lamp in an inert atmosphere. The light intensity was calibrated to $100\,mW/cm^2$.

BIBLIOGRAPHY

[1] A. Kojima, K. Teshima, Y. Shirai, T. Miyasaka, *Journal of the American Chemical Society* **2009**, *131*, 6050–6051.

[2] H. Min, D. Y. Lee, J. Kim, G. Kim, K. S. Lee, J. Kim, M. J. Paik, Y. K. Kim, K. S. Kim, M. G. Kim, T. J. Shin, S. Il Seok, *Nature* **2021**, *598*, 444–450.

[3] G. E. Eperon, S. N. Habisreutinger, T. Leijtens, B. J. Bruijnaers, J. J. van Franeker, D. W. deQuilettes, S. Pathak, R. J. Sutton, G. Grancini, D. S. Ginger, R. A. J. Janssen, A. Petrozza, H. J. Snaith, *ACS Nano* **2015**, *9*, 9380–9393.

[4] X. Yan, W. Fan, F. Cheng, H. Sun, C. Xu, L. Wang, Z. Kang, Y. Zhang, *Nano Today* **2022**, *44*, 101503.

[5] T. S. Sherkar, C. Momblona, L. Gil-Escrig, J. Ávila, M. Sessolo, H. J. Bolink, L. J. A. Koster, *ACS Energy Letters* **2017**, *2*, 1214–1222.

[6] E. A. Alharbi, A. Y. Alyamani, D. J. Kubicki, A. R. Uhl, B. J. Walder, A. Q. Alanazi, J. Luo, A. Burgos-Caminal, A. Albadri, H. Albrithen, M. H. Alotaibi, J.-E. Moser, S. M. Zakeeruddin, F. Giordano, L. Emsley, M. Grätzel, *Nature Communications* **2019**, *10*, DOI 10.1038/s41467-019-10985-5.

[7] W. Shen, Y. Dong, F. Huang, Y.-B. Cheng, J. Zhong, *Materials Reports: Energy* **2021**, *1*, 100060.

[8] Y. Huang, Y. Jiang, S. Zou, Z. Zhang, J. Jin, R. He, W. Hu, S. Ren, D. Zhao, *ACS Applied Materials & Interfaces* **2023**, *15*, 15775–15784.

[9] J. Ren, T. Liu, B. He, G. Wu, H. Gu, B. Wang, J. Li, Y. Mao, S. Chen, G. Xing, *Small* **2022**, *18*, 2203536.

[10] C. C. Stoumpos, D. H. Cao, D. J. Clark, J. Young, J. M. Rondinelli, J. I. Jang, J. T. Hupp, M. G. Kanatzidis, *Chemistry of Materials* **2016**, *28*, 2852–2867.

[11] E. Kirstein, E. A. Zhukov, D. R. Yakovlev, N. E. Kopteva, C. Harkort, D. Kudlacik, O. Hordiichuk, M. V. Kovalenko, M. Bayer, *Nano Letters* **2022**, *23*, 205–212.

[12] M. Dyksik, S. Wang, W. Paritmongkol, D. K. Maude, W. A. Tisdale, M. Baranowski, P. Plochocka, *The Journal of Physical Chemistry Letters* **2021**, *12*, 1638–1643.

[13] Y. Zhang, Y. Liu, Z. Xu, H. Ye, Q. Li, M. Hu, Z. Yang, S. (Liu, *Journal of Materials Chemistry C* **2019**, *7*, 1584–1591.

[14] C. Chen, J. Liang, J. Zhang, X. Liu, X. Yin, H. Cui, H. Wang, C. Wang, Z. Li, J. Gong, Q. Lin, W. Ke, C. Tao, B. Da, Z. Ding, X. Xiao, G. Fang, *Nano Energy* **2021**, *90*, 106608.

[15] Y. Xu, K.-J. Jiang, P. Wang, W.-M. Gu, G.-H. Yu, X. Zhou, Y. Song, *New Journal of Chemistry* **2022**, *46*, 2259–2265.

[16] Y. Du, D. Zhu, Q. Cai, S. Yuan, G. Shen, P. Dong, C. Mu, Y. Wang, X.-C. Ai, *The Journal of Physical Chemistry C* **2022**, *126*, 3351–3358.

[17] H. Lai, B. Kan, T. Liu, N. Zheng, Z. Xie, T. Zhou, X. Wan, X. Zhang, Y. Liu, Y. Chen, *Journal of the American Chemical Society* **2018**, *140*, 11639–11646.

[18] Z. Xu, L. Li, X. Dong, D. Lu, R. Wang, W.-J. Yin, Y. Liu, *Nano Letters* **2022**, *22*, 2874–2880.

[19] X. Zhao, J. Dong, D. Wu, J. Lai, C. Y. Xu, Y. Yao, X. Yang, X. Tang, Q. Song, *Solar RRL* **2022**, *6*, 2200078.

[20] I. C. Smith, E. T. Hoke, D. Solis-Ibarra, M. D. McGehee, H. I. Karunadasa, *Angewandte Chemie* **2014**, *126*, 11414–11417.

[21] N. Ashurov, B. L. Oksengendler, S. Maksimov, S. Rashiodva, A. R. Ishteev, D. S. Saranin, I. N. Burmistrov, D. V. Kuznetsov, A. A. Zakhisov, *Modern Electronic Materials* **2017**, *3*, 1–25.

[22] T. Wang, Y. Fu, L. Jin, S. Deng, D. Pan, L. Dong, S. Jin, L. Huang, *Journal of the American Chemical Society* **2020**, *142*, 16254–16264.

[23] I. Osaka, *Polymer Journal* **2014**, *47*, 18–25.

[24] S. Otep, Y.-C. Lin, H. Matsumoto, T. Mori, K.-H. Wei, T. Michinobu, *Organic Electronics* **2020**, *87*, 105986.

[25] H. Chan, *Progress in Polymer Science* **1998**, *23*, 1167–1231.

[26] E. H. Jung, N. J. Jeon, E. Y. Park, C. S. Moon, T. J. Shin, T.-Y. Yang, J. H. Noh, J. Seo, *Nature* **2019**, *567*, 511–515.

[27] H. Xie, J. Liu, X. Yin, Y. Guo, D. Liu, G. Wang, W. Que, *Colloids and Surfaces A: Physicochemical and Engineering Aspects* **2022**, *635*, 128072.

[28] N. Y. Nia, M. Bonomo, M. Zendehdel, E. Lamanna, M. M. H. Desoky, B. Paci, F. Zurlo, A. Generosi, C. Barolo, G. Viscardi, P. Quagliotto, A. D. Carlo, *ACS Sustainable Chemistry & Engineering* **2021**, *9*, 5061–5073.

[29] D. Xu, Z. Gong, Y. Jiang, Y. Feng, Z. Wang, X. Gao, X. Lu, G. Zhou, J.-M. Liu, J. Gao, *Nature Communications* **2022**, *13*, DOI 10.1038/s41467-022-34768-7.

[30] K. Heinze, H. Lang, *Organometallics* **2013**, *32*, 5623–5625.

[31] M. Rosenblum, R. B. Woodward, *Journal of the American Chemical Society* **1958**, *80*, 5443–5449.

[32] M. Rosenblum, W. G. Howells, *Journal of the American Chemical Society* **1962**, *84*, 1167–1172.

[33] A. Paul, R. Borrelli, H. Bouyanfif, S. Gottis, F. Sauvage, *ACS Omega* **2019**, *4*, 14780–14789.

[34] D. Bao, B. Millare, W. Xia, B. G. Steyer, A. A. Gerasimenko, A. Ferreira, A. Contreras, V. I. Vullev, *The Journal of Physical Chemistry A* **2009**, *113*, 1259–1267.

[35] S. Rodriguez-Gonzalez, Z. Xie, O. Galangau, P. Selvanathan, L. Norel, C. V. Dyck, K. Costuas, C. D. Frisbie, S. Rigaut, J. Cornil, *The Journal of Physical Chemistry Letters* **2018**, *9*, 2394–2403.

[36] C. V. Dyck, M. A. Ratner, *The Journal of Physical Chemistry C* **2017**, *121*, 3013–3024.

[37] Y. Zhang, S. Soni, T. L. Krijger, P. Gordiichuk, X. Qiu, G. Ye, H. T. Jonkman, A. Herrmann, K. Zojer, E. Zojer, R. C. Chiechi, *Journal of the American Chemical Society* **2018**, *140*, 15048–15055.

[38] Y. Liu, X. Qiu, S. Soni, R. C. Chiechi, *Chemical Physics Reviews* **2021**, *2*, 021303.

[39] C. A. Nijhuis, W. F. Reus, J. R. Barber, M. D. Dickey, G. M. Whitesides, *Nano Letters* **2010**, *10*, 3611–3619.

[40] N. K. Gupta, T. Schultz, S. K. Karuppannan, A. Vilan, N. Koch, C. A. Nijhuis, *Physical Chemistry Chemical Physics* **2021**, *23*, 13458–13467.

[41] C. A. Nijhuis, W. F. Reus, G. M. Whitesides, *Journal of the American Chemical Society* **2010**, *132*, 18386–18401.

[42] C. A. Nijhuis, W. F. Reus, G. M. Whitesides, *Journal of the American Chemical Society* **2009**, *131*, 17814–17827.

[43] L. Yuan, N. Nerngchamnong, L. Cao, H. Hamoudi, E. del Barco, M. Roemer, R. K. Sriramula, D. Thompson, C. A. Nijhuis, *Nature Communications* **2015**, *6*, DOI 10.1038/ncomms7324.

[44] H. C. Brown, B. C. S. Rao, *Journal of the American Chemical Society* **1956**, *78*, 2582–2588.

[45] G. S. Mohammad-Pour, K. O. Hatfield, D. C. Fairchild, K. Hernandez-Burgos, J. Rodríguez-López, F. J. Uribe-Romo, *Journal of the American Chemical Society* **2019**, *141*, 19978–19982.

[46] Z. Chen, L. Han, S.-K. Tian, *Organic Letters* **2017**, *19*, 5852–5855.

[47] E. I. Klimova, T. Klimova, L. V. Bakinovsky, M. M. García, *Journal of Organometallic Chemistry* **2006**, *691*, 507–513.

[48] P. M. García-Barrantes, G. V. Lamoureux, A. L. Pérez, R. N. García-Sánchez, A. R. Martínez, A. S. Feliciano, *European Journal of Medicinal Chemistry* **2013**, *70*, 548–557.

[49] J. Lubach, W. Drenth, *Recueil des Travaux Chimiques des Pays-Bas* **1973**, *92*, 586–592.

[50] V. M. Fomin, A. V. Markin, *Journal of Thermal Analysis and Calorimetry* **2008**, *92*, 985–987.

[51] J. Hurvois, C. Moinet, *Journal of Organometallic Chemistry* **2005**, *690*, 1829–1839.

[52] C. G. Armstrong, R. W. Hogue, K. E. Toghill, *Journal of Electroanalytical Chemistry* **2020**, *872*, 114241.

[53] P. T. N. Nonjola, U. Siegert, J. C. Swarts, *Journal of Inorganic and Organometallic Polymers and Materials* **2015**, *25*, 376–385.